HySEA model. Landslide Benchmarking Results

J. Macías[1], C. Escalante[1], M.J. Castro[1], J.M. González-Vida[2], and S. Ortega[3]

[1]Departamento de A. M., E. e I. O. y Matemática Aplicada, Facultad de Ciencias, Universidad de Málaga (UMA), Campus de Teatinos s/n, 29080 Málaga, Spain
[2]Departamento de Matemática Aplicada, Escuela de Ingenierías Industriales, UMA
[3]Unit of Numerical Methods, SCAI, UMA

July 28, 2017

Abstract

In this document we describe the application of two models of the HySEA family, the Landslide and the Multilayer-HySEA models, to the study of the benchmark test cases established for the NTHMP Landslide Benchmark Workshop, held in January 2017 at Galveston. The Multilayer-HySEA model is used to perform the first five benchmark problems, dealing with laboratory experiments. This model consists in a hybrid finite volume/finite difference implementation of a non-hydrostatic multilayer model. The Landslide-HySEA model is used to simulate the field case of Port Valdez (benchmark problem 7). It implements a fully coupled shallow-water/Savage-Hutter model. Due to its more complex setup, benchmark 6 remains as the only one we have not performed using a HySEA model yet. A brief description of models equations and numerical schemes are included. Then, results for Benchmarks 1-5 and 7 are presented.

1 Model Background

HySEA (Hyperbolic Systems and Efficient Algorithms) software consists of a family of geophysical codes based on either single layer, two-layer stratified systems or multilayer shallow water models. HySEA codes (https://edanya.uma.es/hysea) have been developed by EDANYA Group[1] from the University of Malaga (UMA) for more than a decade and they are in continuous evolution and upgrading. Initially, the software was developed and the numerical algorithms implemented published under no particular name. Several developments have been published in peer-review international journals since 2005 where different analytical and experimental test cases have been presented. Some of these model developments can be found in Castro el al. (2005, 2006, 2008, 2012a), Gallardo et al. (2007) and de la Asunción et al. (2013). In September 2013, at ITS 2013, held at Göcek (Turkey) the ensemble of all the codes was named as HySEA for the very first time, and Landslide-HySEA (applied to an aerial landslide) and Tsunami-HySEA were presented in the two separate contributions González-Vida et al. (2013) and Macías et al. (2013b), respectively. The work in Macías et al. (2015), in this case for a submarine landslide, it is the first peer-review paper where a HySEA code is named as such.

Tsunami-HySEA is the numerical model specifically designed for tsunami simulations. It combines robustness, reliability and good accuracy in a model based on a GPU faster than real time (FTRT) implementation. It has been severely tested and, in particular, has passed all tests in Synolakis et al. (2008), but also other laboratory tests and proposed benchmark problems. Recently, much effort has been put on validating and verifying Tsunami-HySEA model under NTHMP stardards. First for propagation and inundation (Macías et al., 2017b) and then for currents (Macías et al,

[1]https://www.uma.es/edanya/

2017a, c). Concerning landslide-generated tsunamis, a stratified two-layer Savage-Hutter shallow water model, the Landslide-HySEA model, was implemented based on Fernández-Nieto et al. (2008) and incorporated to the HySEA family. Validation of this code, comparing numerical results with the laboratory experiments of Heller and Hager (2011) and Fritz et al. (2001) can be found at Sánchez-Linares (2011). A milestone in the validation process of this code consisted in the numerical simulation of the Lituya Bay 1958 mega-tsunami with real topo-bathymetric data (González-Vida et al. 2017). This validation was carried out under a research contract with PMEL/NOAA. The result of this project leads NCTR to adopt Landslide-HySEA as the numerical code used to generate initial conditions for the MOST model to be initialized in the case of landslide-generated tsunami scenarios. A new joint work with PMEL/NOAA consisted in the simulation of a hypothesized submarine landslide at Hudson Canyon. This numerical work was carried out in 2013, and a technical memorandum was written (de la Asunción et al. 2013). Finally, a joint work with the Dept Estratigrafia, Paleontologia i Geociènces Marines (GRC Geociènces Marines, Universitat de Barcelona) on a simulation study of the tsunamigenic potential of four submarine landslides located on the Ibiza Channel in the Western Mediterranean Sea can be found at Iglesias (2015) and will appear in Iglesias et al. (2017).

2 Model Equations

2.1 Landslide-HySEA model

The Landslide-HySEA tsunami model implements the natural 2D extension of the 1D two-layer Savage-Hutter model presented in Fernández-Nieto et al. (2008) where Cartesian coordinates are used instead of local coordinates at each point of the 2D domain and where no anisotropy effects are taken into account in the normal stress tensor of the solid phase. The propagation and inundation components of HySEA models have been fully validated using all of NOAA's National Tsunami Mitigation Program (NTHMP) mandatory benchmarks (Macías et al., 2017a, b, c). The mathematical model landslide generated tsunamis consists of two systems of equations that are coupled: the model for the slide material is represented by a Savage-Hutter type of model (Savage and Hutter, 1989) and the water dynamics model represented by the shallow water equations (see Fernández-Nieto et al., 2008). One of the most important features of the model is that both the dynamics of the sedimentary fluidized material and the seawater layer are coupled and each of these two phases influences the other one instantly and they are computed simultaneously. These coupled effects were first studied in a 1D model by Jiang and Leblond (1992), who concluded that these effects are significant for cases of smaller slide material density and shallower waters. Those conditions are verified for aerial and submarine landslides in fjords, lakes or coastal areas. The importance of numerically treating in a coupled mode phenomena that are physically coupled have been studied, for example, in Castro et al. (2011a) for the case of two layer shallow water fluids, and in Cordier et al. (2011) for sediment transport models. An uncoupled numerical treatment of these systems may generate spurious oscillations at the water surface or the interface.

The mathematical model implemented in the Landslide-HySEA code consists of a stratified media of two layers, the first layer is composed of a homogeneous inviscid fluid with constant density ρ_1, (seawater here) and the second layer represents the fluidized granular material with density ρ_s and porosity ψ_0. We assume that the mean density of the fluidized debris is constant and equals to $\rho_2 = (1-\psi_0)\rho_s + \psi_0\rho_1$ and that the two fluids (water and fluidized debris) are immiscible.

For sake of simplicity the 1D system is written here, and the 2D extension is straightforward (see Macías et al. 2015):

$$\begin{cases} \dfrac{\partial h_1}{\partial t} + \dfrac{\partial q_1}{\partial x} = 0 \\ \dfrac{\partial q_1}{\partial t} + \dfrac{\partial}{\partial x}\left(\dfrac{q_1^2}{h_1} + \dfrac{g}{2}h_1^2\right) = -gh_1\dfrac{\partial h_2}{\partial x} + gh_1\dfrac{dH}{dx} + S_{i_1} \\ \dfrac{\partial h_2}{\partial t} + \dfrac{\partial q_2}{\partial x} = 0 \\ \dfrac{\partial q_2}{\partial t} + \dfrac{\partial}{\partial x}\left(\dfrac{q_2^2}{h_2} + \dfrac{g}{2}h_2^2\right) = -g\dfrac{\rho_1}{\rho_2}h_2\dfrac{\partial h_1}{\partial x} + gh_2\dfrac{dH}{dx} + S_{i_2} + \tau, \end{cases} \tag{1}$$

In these equations, index 1 corresponds to the upper layer and index 2 to the second layer. $h_i(x,t)$, $i = 1, 2$ is the layer thickness at each point at time t, therefore h_2 stands for the thickness of the slide layer material; $H(x)$ is the fixed bathymetry at each point measured from a given reference level, $q_i(x,t)$, $i = 1, 2$ is the discharge and is related to the mean velocity by the equation $u_i(x,t) = q_i(x,t)/h_i(x,t)$, g is the gravitational acceleration and r is the ratio of densities $r = \rho_1/\rho_2$.

τ is a parametrization of the Coulomb friction term and it is defined by:

$$\tau = \begin{cases} gh_2(1 - \frac{\rho_2}{\rho_1})\frac{u_2}{|u_2|}\tan(\delta_0) & \text{if } \tau > \sigma_c \\ u_2 = 0 & \text{otherwise} \end{cases}$$

with

$$\sigma_c = gh_2(1 - \frac{\rho_1}{\rho_2})\tan(\delta_0).$$

being α the Coulomb friction angle. The above expression models the fact that a critical slope is needed to trigger the slide movement.

Finally, S_{i_1} and S_{i_2} contain the friction terms between layers that are parametrized by quadratic friction laws (see Macías et al. 2015).

Note that this model reduces to the usual nonlinear shallow-water system when the layer of granular material is not present or when it has zero velocity and this layer reaches equilibrium. Therefore, the model can be used to numerically reproduce the different stages of a landslide tsunami simulation: the landslide tsunami generation, wave propagation and, finally, coastline inundation and run-up height reached by the tsunami wave.

2.2 Multilayer-HySEA model

The previous model it is difficult to approximate due to the presence of the coupling pressure terms. Moreover, it makes also difficult to consider its natural extension to non-hydrostatic flows. For this reason, when trying to include dispersion in our models, we consider first the following equivalent formulation of (1):

$$\begin{cases} \dfrac{\partial h_1}{\partial t} + \dfrac{\partial q_1}{\partial x} = 0 \\ \dfrac{\partial q_1}{\partial t} + \dfrac{\partial}{\partial x}\left(\dfrac{q_1^2}{h_1}\right) + gh_1\dfrac{\partial \eta_1}{\partial x} = S_{i_1} \\ \dfrac{\partial h_2}{\partial t} + \dfrac{\partial q_2}{\partial x} = 0 \\ \dfrac{\partial q_2}{\partial t} + \dfrac{\partial}{\partial x}\left(\dfrac{q_2^2}{h_2}\right) + gh_2\dfrac{\partial}{\partial x}\left((1-r)\eta_2 + r\eta_1\right) = S_{i_2} + \tau, \end{cases} \tag{2}$$

where η_1 is the free surface and it is given by $\eta_1 = h_1 + h_2 - H$; η_2 is the interface between the fluid and the granular material and it is defined by $\eta_2 = h_2 - H$ and $r = \frac{\rho_1}{\rho_2}$.

Now, if $\partial_x \eta_1$ is neglected in the momentum equation of the granular material, that is, the fluctuation of pressure due to the variations of the free-surface is neglected in the momentum equation of the granular material, then the following weakly-coupled system could be obtained:

$$\text{S-W system} \begin{cases} \dfrac{\partial h_1}{\partial t} + \dfrac{\partial q_1}{\partial x} = 0 \\ \dfrac{\partial q_1}{\partial t} + \dfrac{\partial}{\partial x}\left(\dfrac{q_1^2}{h_1}\right) + g h_1 \dfrac{\partial \eta_1}{\partial x} = S_{i_1} \end{cases}$$

$$\text{S-H system} \begin{cases} \dfrac{\partial h_2}{\partial t} + \dfrac{\partial q_2}{\partial x} = 0 \\ \dfrac{\partial q_2}{\partial t} + \dfrac{\partial}{\partial x}\left(\dfrac{q_2^2}{h_2}\right) + (1-r) g h_2 \dfrac{\partial \eta_2}{\partial x} = S_{i_2} + \tau, \end{cases} \tag{3}$$

where the first system is the standard one layer shallow-water system and the second one is the one layer reduced-gravity Savage-Hutter model, that takes into account that the granular landslide is underwater. Note that the previous system could be also adapted to simulate subaerial/submarine landslides by a suitable treatment of the variation of the gravity terms. Under this formulation, it is now straightforward to improve the numerical model for the fluid phase by including non-hydrostatic effects.

The Multilayer-HySEA model implements one of the multi-layer non-hydrostatic models of the family introduced and described in Fernández-Nieto et al (2016). The governing equations, obtained by a process of depth-averaging, correspond to a semi-discretization with respect to the vertical variable of the Euler equations. Total pressure is decomposed into a sum of hydrostatic and non-hydrostatic pressures. In this process, vertical velocities are assumed to have a linear vertical profile while the horizontal velocities are assumed to have a constant vertical profile. The proposed model admits an exact energy balance, and when the number of layers increases, the linear dispersion relation of the linear model converges to the same of Airy's theory. The model proposed in Fernández-Nieto et al (2016) can be written in compact form as

$$\begin{cases} \partial_t h + \partial_x (hu) = 0, \\ \partial_t (hu_\alpha) + \partial_x \left(h u_\alpha^2 + \dfrac{1}{2} g h^2 \right) - g h \partial_x H + u_{\alpha+1/2} \Gamma_{\alpha+1/2} - u_{\alpha-1/2} \Gamma_{\alpha-1/2} = -h \left(\partial_x p_\alpha + \sigma_\alpha \partial_z p_\alpha \right) - \tau, \\ \partial_t (h w_\alpha) + \partial_x (h u_\alpha w_\alpha) + w_{\alpha+1/2} \Gamma_{\alpha+1/2} - w_{\alpha-1/2} \Gamma_{\alpha-1/2} = -h \partial_z p_\alpha, \\ \partial_x u_{\alpha-1/2} + \sigma_{\alpha-1/2} \partial_z u_{\alpha-1/2} + \partial_z w_{\alpha-1/2} = 0, \end{cases} \tag{4}$$

where, for $\alpha \in \{1,\ 2, \ldots, L\}$

$$u_{\alpha+1/2} = \frac{1}{2}\left(u_{\alpha+1} + u_\alpha\right),\ \partial_z u_{\alpha+1/2} = \frac{1}{h\Delta s}\left(u_{\alpha+1} - u_\alpha\right),$$

$$w_{\alpha+1/2} = \frac{1}{2}\left(w_{\alpha+1} + w_\alpha\right),\ \partial_z w_{\alpha+1/2} = \frac{1}{h\Delta s}\left(w_{\alpha+1} - w_\alpha\right).$$

$$p_\alpha = \frac{1}{2}\left(p_{\alpha+1/2} + p_{\alpha-1/2}\right),\ \partial_z p_\alpha = \frac{1}{h\Delta s}\left(p_{\alpha+1/2} - p_{\alpha-1/2}\right),$$

$$\sigma_\alpha = \partial_x \left(H - h\Delta s(\alpha - 1/2)\right),\ \sigma_{\alpha-1/2} = \partial_x \left(H - h\Delta s(\alpha - 1)\right),$$

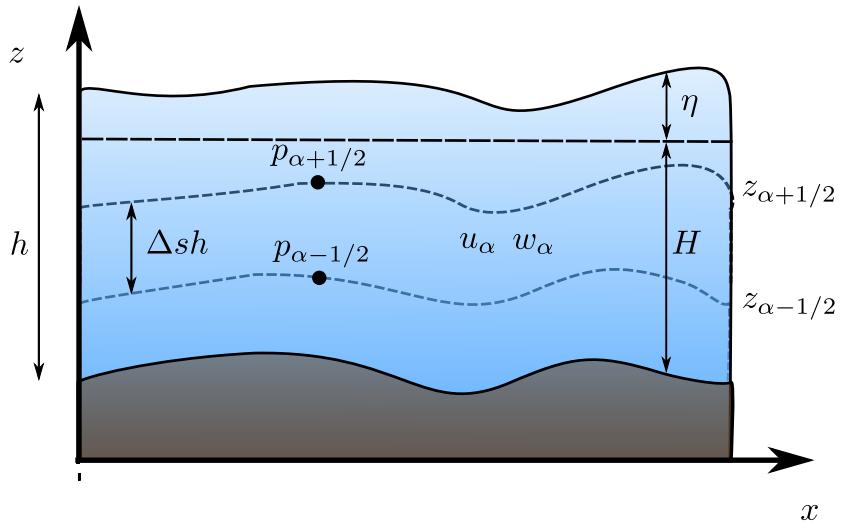

Figure 1: Schematic diagram describing the multilayer system

As depicted in Figure 1, the flow depth h is split along the vertical axis into $L \geq 1$ layers and $\Delta s = 1/L$. u_α and w_α are the depth averaged velocities in the x and z direction respectively, t is time and g is gravitational acceleration. $p_{\alpha+1/2}$ is the non-hydrostatic pressure at the interface $z_{\alpha+1/2}$. The surface elevation measured from the still-water level is $\eta = h - H$, where H is the still water depth. Finally, τ is a friction law term and terms $\Gamma_{\alpha+1/2}$ account for the mass transfer across interfaces and are defined by

$$\Gamma_{\alpha+1/2} = \sum_{\beta=\alpha+1}^{L} \partial_x \left(h \Delta s \left(u_\beta - \bar{u} \right) \right), \ \bar{u} = \sum_{\alpha=1}^{L} \Delta s u_\alpha$$

In order to close the system, the following boundary conditions are considered

$$p_{L+1/2} = 0, \ u_0 = 0, \ w_0 = -\partial_t H.$$

Note that the motion of the bottom surface can be taken into account as a boundary condition, imposing $w_0 \neq 0$. Therefore, this model can simulate the interaction with a slide in the case that the motion of the bottom is prescribed by a function, given by set of data, or simulated by a numerical model. Here we are going to consider tests where either the motion of the bathymetry is given by a known function (solid block) or it is simulated by a Savage-Hutter model (granular material).

3 Numerical Solution Method

The discretization of system (1) is performed by an explicit first order IFCP Finite Volume Scheme where the discretization of the Coulomb friction term is performed following Fernández-Nieto et al. (2008), (see Fernández-Nieto et al. (2011) for details on the stability, convergence and efficiency of the numerical scheme). The resulting scheme has been implemented in Graphics Processors Units (GPUs) using CUDA, achieving a speed-up of two-order of magnitude compared to a conventional CPU implementation (see Castro et al. (2011b) for a review and de la Asunción et al. (2012)). This methodology allows us to considerably improve the efficiency of the algorithm as well as the size of the discrete problems that can be solved.

The discretization of system (4) becomes more difficult. Here we consider the natural extension of the procedure described in Escalante et al (2017), where a splitting technique has been proposed. Thus, in the first step, the non-conservative hyperbolic system underlying system (4) given by

$$\partial_t \mathbf{U} + \partial_x \mathbf{F}_{SW}(\mathbf{U}) + \mathbf{B}_{SW}(\mathbf{U})\partial_x \mathbf{U} = \mathbf{G}_{SW}(\mathbf{U})\partial_x H \tag{5}$$

is discretized by a second order finite volume PVM positive-preserving well-balanced path-conservative method (Fernández-Nieto et al 2011), where

$$\mathbf{U} = \begin{pmatrix} h \\ hu_1 \\ \vdots \\ hu_L \\ hw_1 \\ \vdots \\ hw_L \end{pmatrix}, \ \mathbf{F}_{SW}(\mathbf{U}) = \begin{pmatrix} hu \\ \frac{hu_1^2}{h} + \frac{1}{2}gh^2 \\ \vdots \\ \frac{hu_L^2}{h} + \frac{1}{2}gh^2 \\ hu_1 w_1 \\ \vdots \\ hu_L w_L \end{pmatrix}, \ \mathbf{G}_{SW}(\mathbf{U}) = \begin{pmatrix} 0 \\ gh \\ \vdots \\ gh \\ 0 \\ \vdots \\ 0 \end{pmatrix}.$$

$\mathbf{B}_{SW}$ is a matrix such $\mathbf{B}_{SW}\partial_x \mathbf{U}$ involves the non-conservative products related to the mass transfer across interfaces that appear at the momentum equations. Next, the non-hydrostatic pressure term $\mathcal{T}_{\mathcal{NH}}(h, h_x, H, H_x, p, p_x)$ given by

$$\mathcal{T}_{\mathcal{NH}}(h, h_x, H, H_x, p, p_x) = - \begin{pmatrix} 0 \\ h\left(\partial_x p_1 + \sigma_1 \partial_z p_1\right) \\ \vdots \\ h\left(\partial_x p_L + \sigma_L \partial_z p_L\right) \\ h\partial_z p_1 \\ \vdots \\ h\partial_z p_L \end{pmatrix},$$

is computed solving an elliptic operator that appears when imposing the continuity equation at each layer, $\mathcal{B}(\mathbf{U}, \mathbf{U}_x, H, H_x) = 0$, where

$$\mathcal{B}(\mathbf{U}, \mathbf{U}_x, H, H_x) = \begin{pmatrix} \partial_x u_{1/2} + \sigma_{1/2}\partial_z u_{1/2} + \partial_z w_{1/2} \\ \vdots \\ \partial_x u_{L-1/2} + \sigma_{L-1/2}\partial_z u_{L-1/2} + \partial_z w_{L-1/2} \end{pmatrix}.$$

The elliptic operator is discretized using standard central finite differences. Let us also point that a common arrangement of the discretized variables is used (see Figure 2). The resulting linear system is solved using an iterative Jacobi method combined with a scheduled relaxation (see Adsuara et al 2016 and Escalante et al 2017).

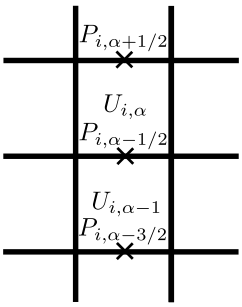

Figure 2: Arragement of discrete variables in the multilayer model discretization algorithm

Finally, when the pressure corrections are computed, the discharges at each layer are updated. The resulting numerical scheme is well-balanced for the water at rest solution and is linearly L^∞-stable under the usual CFL condition related to the hydrostatic system. It is also worth to mention that the numerical scheme is positive preserving. Finally, its extension to 2D is straightforward. In this case, the computational domain is decomposed into subsets with a simple geometry, called cells or finite volumes. The first step of the algorithm adapts well to GPUs architectures as is shown in Castro et al (2011b). Moreover, the compactness of the numerical stencil and the easy parallelization of the Jacobi method makes that the second step can also be implemented on GPUs.

4 Benchmark Problem Comparisons

In this section we present the numerical results obtained with HySEA codes and the comparison with the measured lab data or observations (for BP7). The first five Benchmark Problems (BPs) have been simulated using the Multilayer-HySEA model, which includes non-hydrostatic processes. BP1, 2 and 3 deal with waves generated by the movement of a solid block. 2D submarine for BP1, 3D submarine for BP2, and 3D partially submerged and submarine for BP3. In all these cases a moving bottom condition has been used to modeled the solid block movement. For BP4 and 5, dealing with granular landslides, 2D submarine for BP4 and 2D subaerial for BP5, a one-way coupling between the Multilayer-HySEA model and a Savage-Hutter layer modeling the granular slide is used to reproduce these two experiments. Finally BP7, dealing with a field case at Port Valdez, Alaska, is simulated using Landslide-HySEA model.

4.1 Benchmark Problem 1: Two-dimensional submarine solid block

In this benchmark two items remain undetermined: they are the initialization of the numerical experiment and the second one is how and where and how the moving solid block must stop.

The one-dimensional domain $[-1, 10]$ is discretized with $\Delta x = 0.02\ m$ and the number of layers was set up to 3. Similar results were obtained with more layers. The simulated time was 4 s. CFL was set to 0.9 and $g = 9.81$. Outflow boundary conditions are used. In order to capture turbulent processes, following Ma et al (2012), the complete Navier-Stokes viscous stress tensor is used, where the turbulent kinematic viscosity is estimated by the Smagorinsky subgrid model, with $C_s = 0.2$ (Smagorinsky turbulent coefficient) and $k_s = 0.01$ (bottom roughness height).

First, we would like to stress that we found a bit confusing geometry definition for this benchmark problem, mainly due to the sometimes unclear use of dimension and dimensionless variables, not always consistent with the non-tilde vs tilde notation, respectively. In our presentation at the workshop, we stressed the mismatch we found between provided data and figures in the benchmark description: we were not able to reproduce, with the given data, the figures provided in the document describing the benchmark. To illustrate this fact, we presented the numerical results obtained with the Multilayer-HySEA model that has been adimensionalized in time dividing by $t_0 = 1.677$ and compared them

with the measured data, first adimensionalized using the same value (as should be coherent, but the resulting figure does not agree with the figures provided in the benchmark description) and then using the value $T = t_0 + t_i$ (with t_i the initialization time appearing in the benchmark problem description) to adimensionalize. Here we have compared the numerical results with the lab data adimensionalized using the former value for T.

In Figure 3 comparison of filtered lab measured data with numerical results are presented.

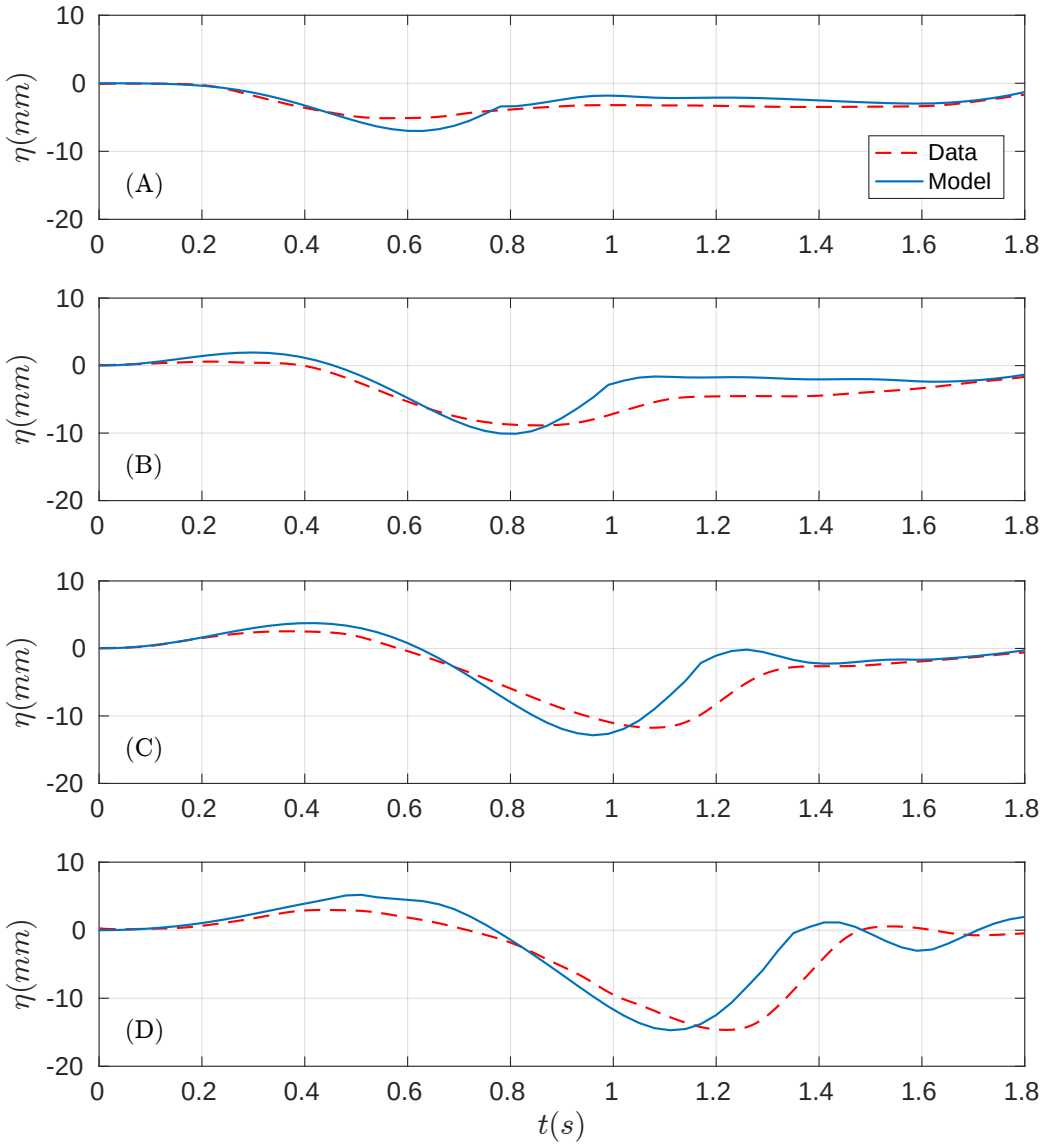

Figure 3: Comparison of filtered data time series (red) and numerical (blue) at wave gauges (A) g_0, (B) g_1, (C) g_2, and (D) g_3.

4.2 Benchmark Problem 2: Three-dimensional submarine solid block

As in BP1, in this benchmark the same two items remain undetermined: initialization and stoping of the solid block. With respect to the described as "numerical artifact" in the questions after the presentation at the workshop, we have determined that this was not a numerical artifact, but the "shadow" of the moving block at surface. The appearance of this bump at surface can be avoided by stopping the solid block earlier and it appears when the block is moved as far as posible ("possible" from a physical point of view, or even "beyond", if doing it numerically). We have numerical experiments and animations of different strategies showing the described behavior.

The two-dimensional domain $[-1, 10] \times [-1.8, 1.8]$ is discretized with $\Delta x = \Delta y = 0.02\ m$ and the number of layers was set up to 3. Similar results were observed using more layers. The simulated time was 4 s. We set the $CFL = 0.9$ and $g = 9.81$. Outflow boundary conditions are imposed at $x = -1,\ x = 10$ and wall boundary conditions at $y = -1.8,\ y = 1.8$.

We present numerical results for two proposed cases (out the seven included in this data set) for $d = 61\,mm$ and $d = 120\,mm$. Figure 4 shows the results for the first case, $d = 61\,mm$, and Figure 5 depicts the results for the second case, $d = 120\,mm$. In this second case measured lab data for gauge G3 were not available.

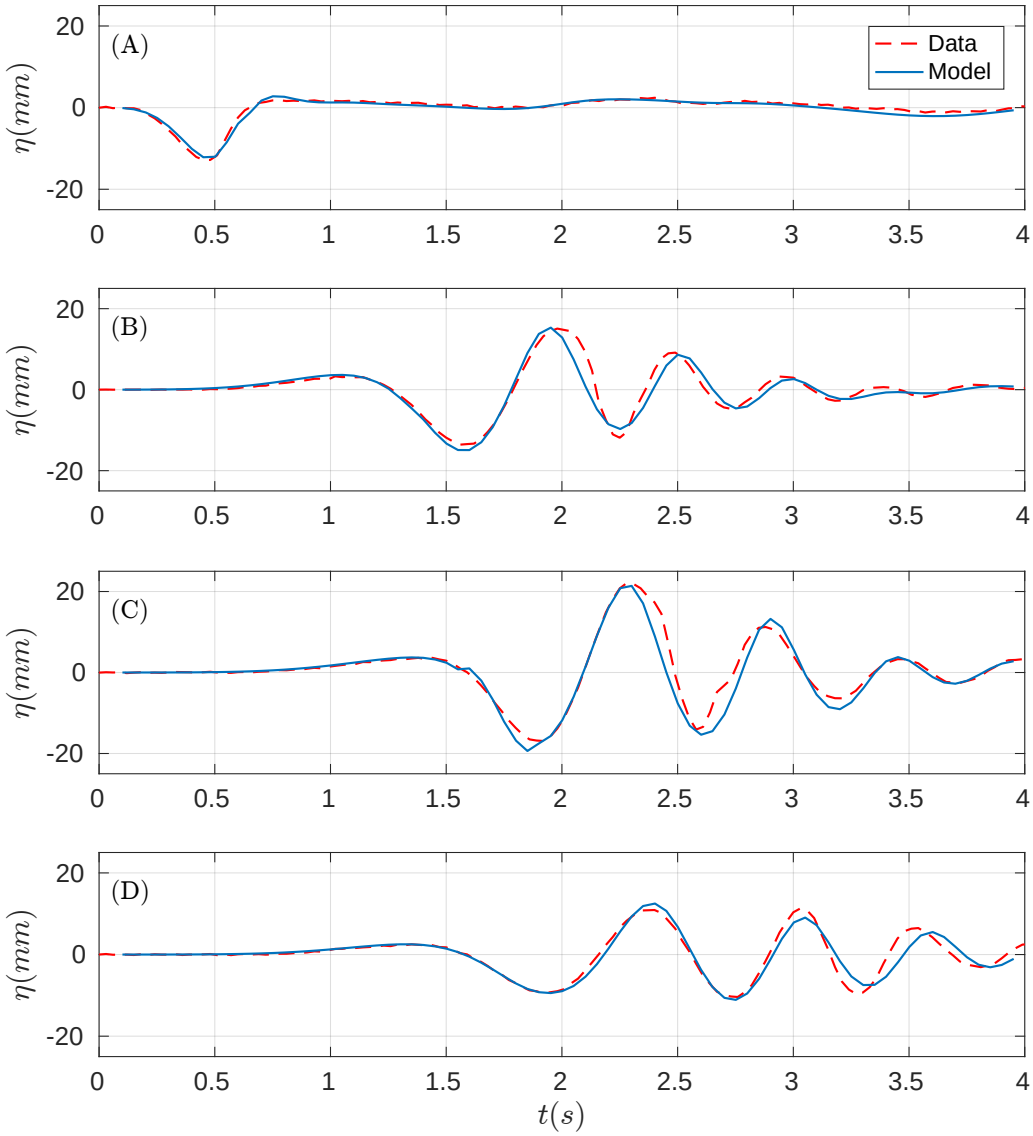

Figure 4: Comparison of data time series (red) and numerical (blue) at wave gauges (A) g_1, (B) g_2, (C) g_3, and (D) g_4 for the case $d = 61\ mm$.

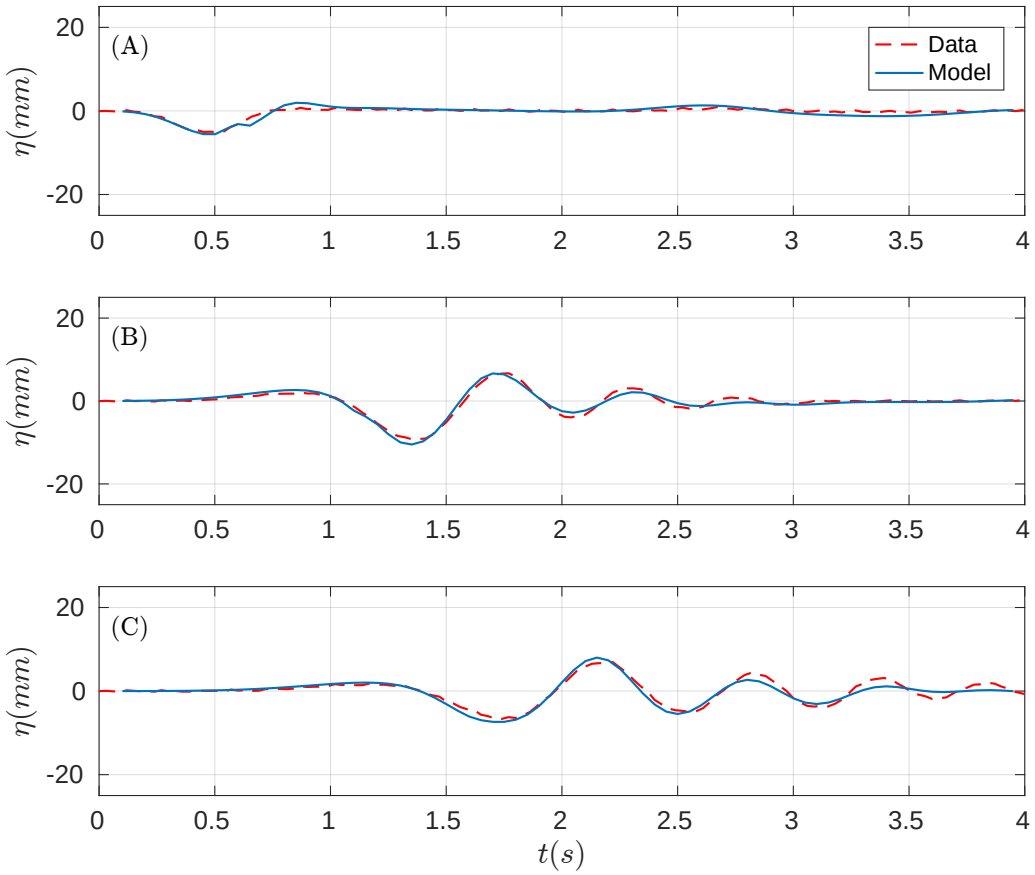

Figure 5: Comparison of data time series (red) and numerical (blue) at wave gauges (A) g_1, (B) g_2, and (C) g_4 for the case $d = 120\ mm$.

4.3 Benchmark Problem 3: Three-dimensional submarine/subaerial triangular solid block

The two-dimensional domain $[-2, 6] \times [-1.85, 1.85]$ is discretized with $\Delta x = 0.02\ m$ and the number of layers was set up to 3. Similar results were observed if more layers are considered. The final time is 4 s, CFL number was set to 0.9 and $g = 9.81$. The same boundary conditions as in the previous case were imposed. In order to capture turbulent processes, as in benchmark 1, the complete Navier-Stokes viscous stress tensor is used with the same subgrid model and coefficients.

Figures 6 and 7 show the numerical results obtained for the subaerial test case, first presenting the comparison for the wave gauges (Fig. 6) and the for the runup gauges (Fig. 7) . The same comparison can be found in Figures 8 and 9 for the submerged test case.

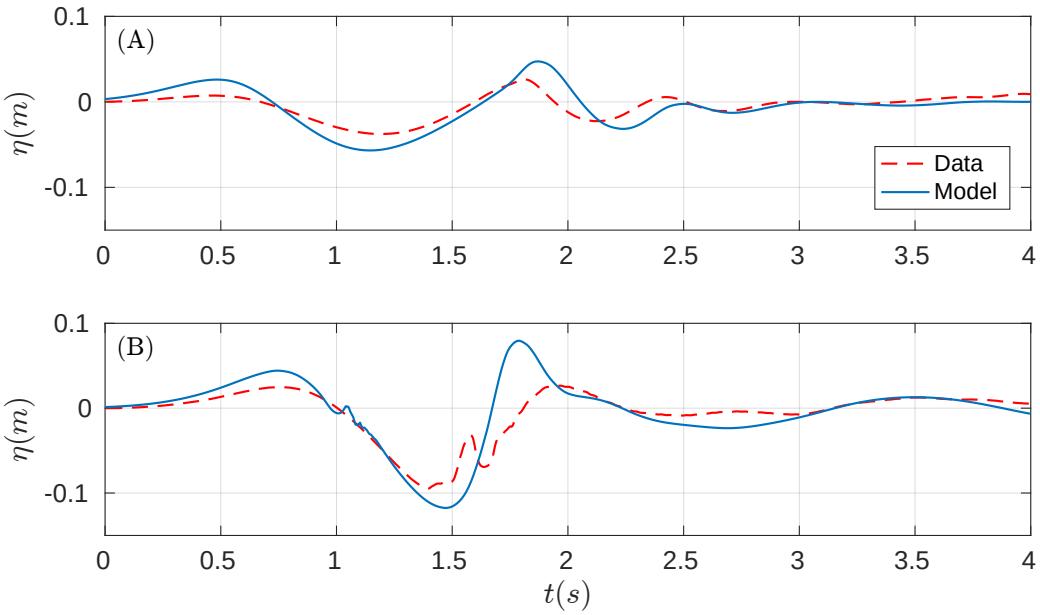

Figure 6: Comparison of data time series (red) and numerical (blue) at wave gauges (A) WG1 and (B) WG2 for the subaerial case.

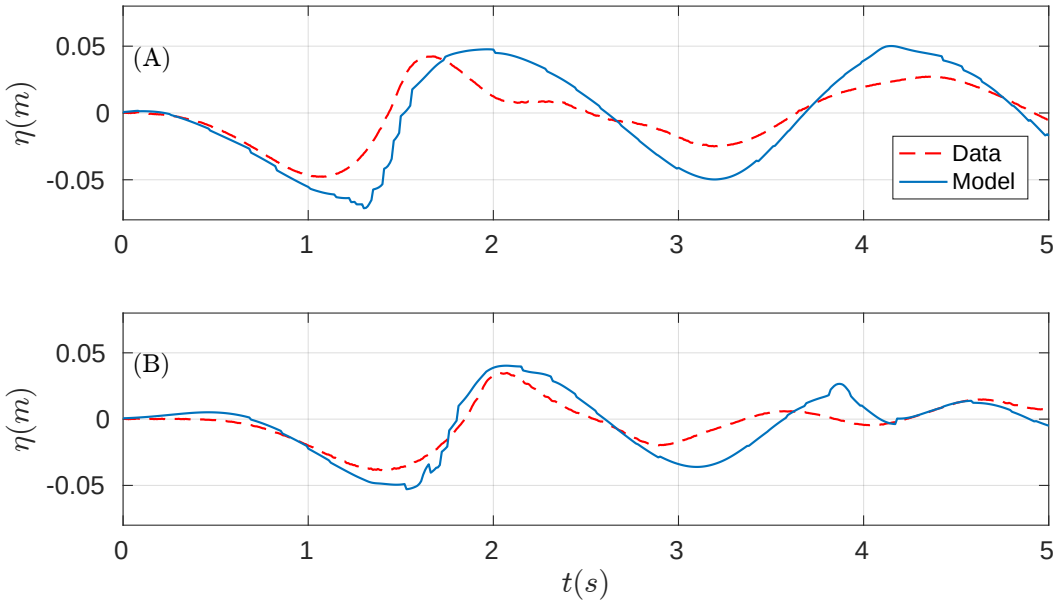

Figure 7: Comparison of data runup time series (red) and numerical (blue) at runup gauges (A) RG2 and (B) RG3 for the subaerial case.

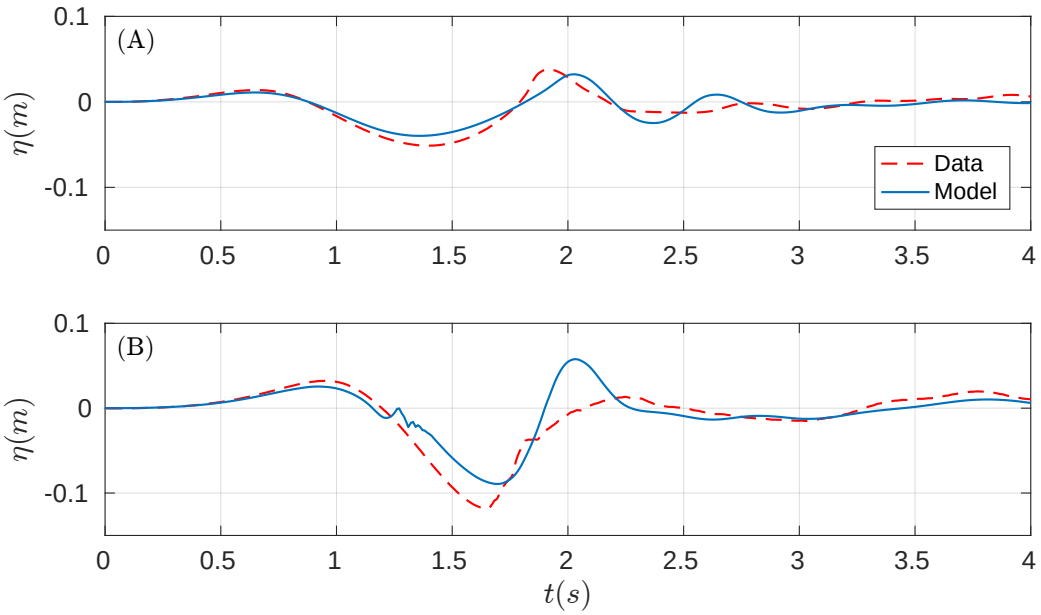

Figure 8: Comparison of data time series (red) and numerical (blue) at wave gauges (A) WG1 and (B) WG2 for the submerged case.

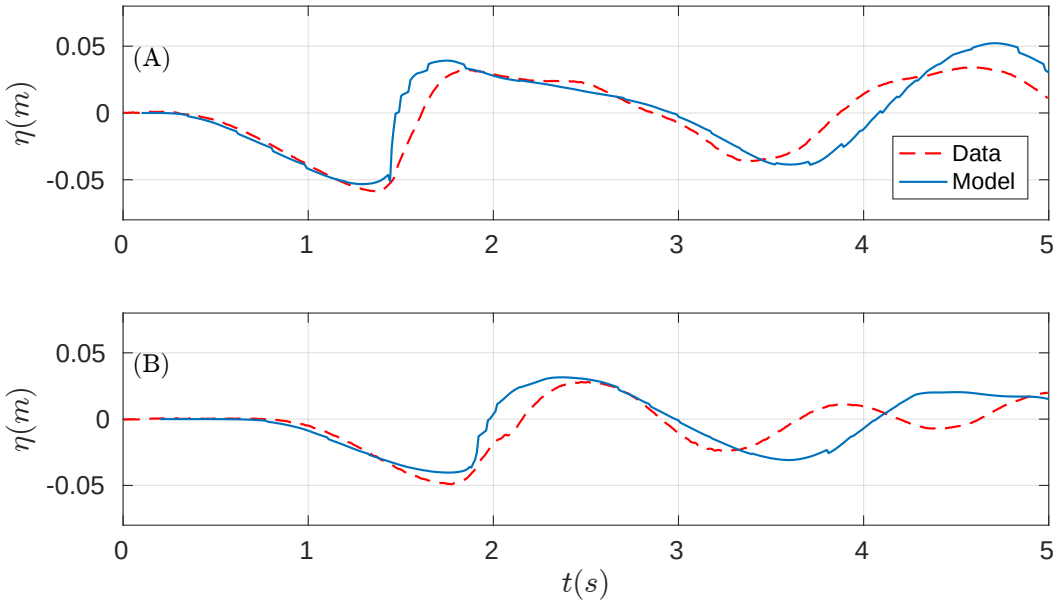

Figure 9: Comparison of data runup time series (red) and numerical (blue) at runup gauges (A) RG2 and (B) RG3 for the submerged case.

4.4 Benchmark Problem 4: Two-dimensional submarine granular slide

For the simulation of the present benchmark problem, a coupled non-hydrostatic multilayer/Savage-Hutter model was used. The resulting model is weakly coupled, and the water feels the moving bottom, but the slide material is not affected by the gradient variations of water surface. The number of layers was set up to 5. Similar results are obtained with less layers, for example 3 as were considered in the previous tests. In this case, the number of layers was increased with the aim of obtaining a similar agreement with measured data as in previous benchmark problems but the numerical results remained similar for a larger number of layers. This may indicate that it is not a question of the dispersive properties of the model (that improve with the number of layers) but more likely due to some missing physics.

The one-dimensional domain $[0, 5.47]$ is discretized with $\Delta x = 0.005\ m$. The final time is 10 s. We set the $CFL = 0.5$ and $g = 9.81$. Wall boundary conditions were imposed. The ratio of densities $r = \dfrac{\rho_s}{\rho_b} = 0.78$, the Coulomb friction was set to $\delta = 12^\circ$ and Manning $n = 0.0002$.

Figure 10 shows the comparison of model results with lab data for the for wave gauges considered. Figure 11 depicts the water free surface and the grain location at several times during the numerical simulation.

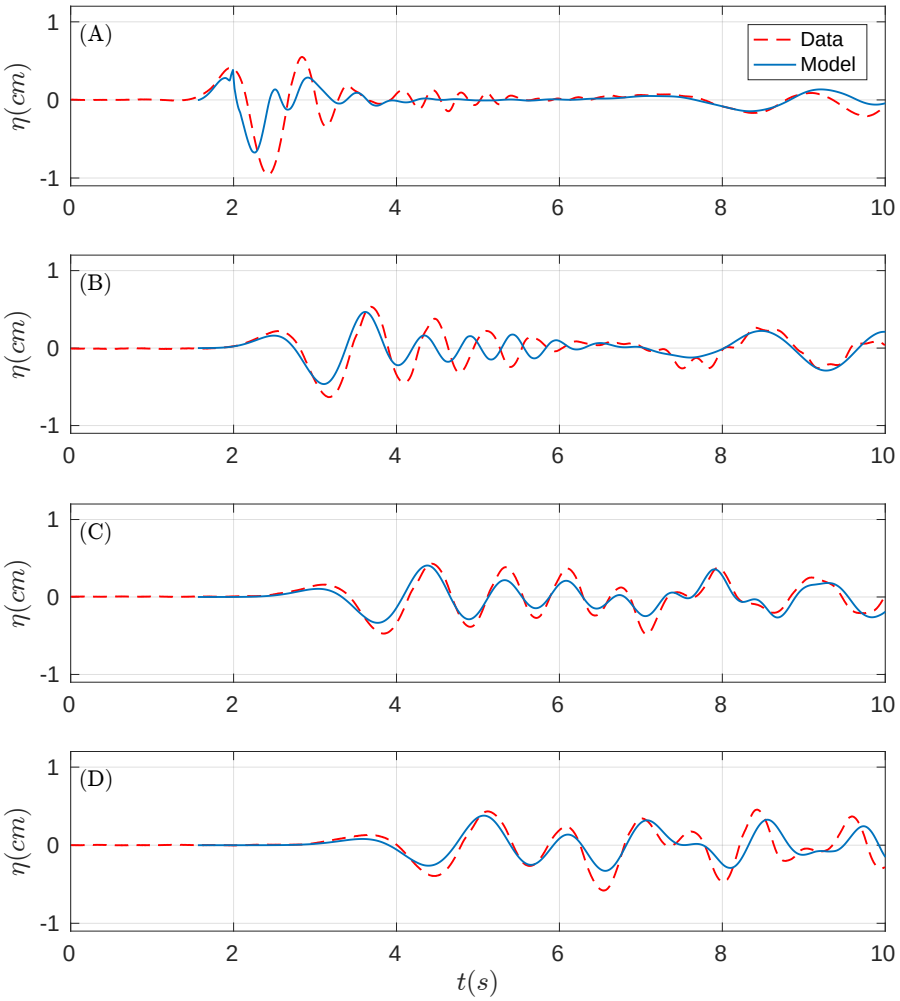

Figure 10: Comparison of data time series (red) and numerical (blue) at wave gauges (A) WG1, (B) WG2, (C) WG3, and (D) WG4.

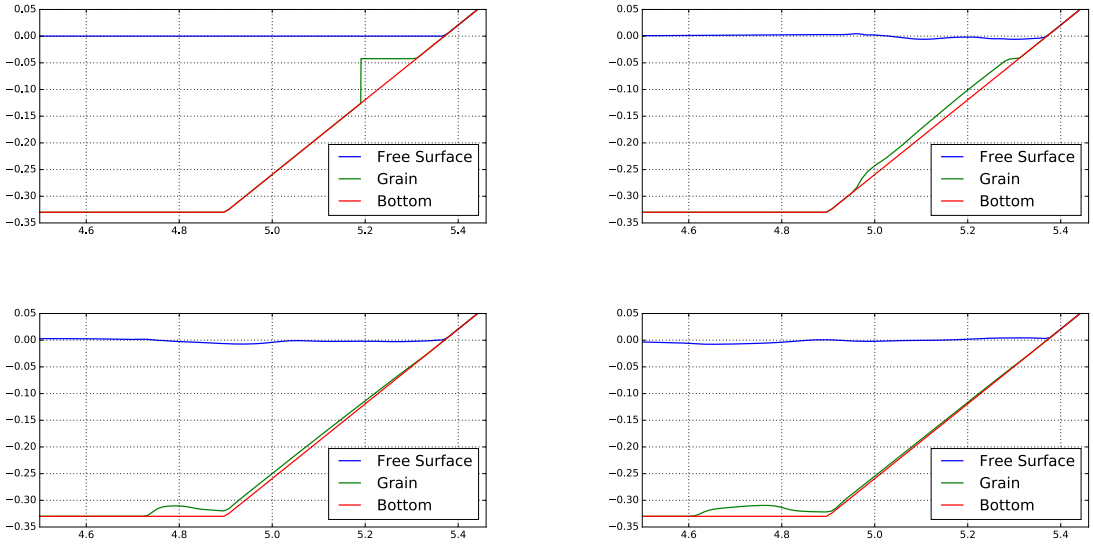

Figure 11: Numerical profiles of the water free surface elevation and the grain layer location at times $t = 0,\ 0.3,\ 0.6,\ 0.9\ s$.

4.5 Benchmark Problem 5: Two-dimensional subaerial granular slide

For this benchmark we use the same model configuration as in the former problem: the Multilayer-HySEA (non-hydrostatic) model coupled with a Savage-Hutter model for the granular material (the latter is the same as the one implemented in the Landslide-HySEA model). The resulting model is weakly coupled, and the water feels the moving bottom, but the slide material is not affected by the gradient variations of water surface. The number of layers was set up to 3.

The one-dimensional domain $[0, 2.2]$ is discretized with $\Delta x = 0.003\ m$. The simulation time is 2.5 s. We set the $CFL = 0.9$ and $g = 9.81$. Wall boundary conditions were imposed. The ratio of densities $r = \dfrac{\rho_s}{\rho_b} = 0.6$, the Coulomb friction was set to $\delta = 12°$ and Manning $n = 0.0001$.

Figure 12 shows the comparison for Case 1 ($D = 1.5$ mm, $H = 14.8$ cm and $L = 11$ cm). Figure 13 shows the comparison for Case 2 ($D = 10$ mm, $H = 15$ cm and $L = 13.5$ cm). Figure 14 depicts the free surface elevation and the granular layer location at several times for Case 1. It can be observed that the agreement with lab data is much better for Case 1 than for Case 2 and also that this agreement is also better for gauges located further from the slide. This latter behavior can be explained as a consequence of the fact that the hydrodynamic component is much better resolved and simulated than the morphodynamic component (the movement of the slide material), obviously much more difficult to reproduce.

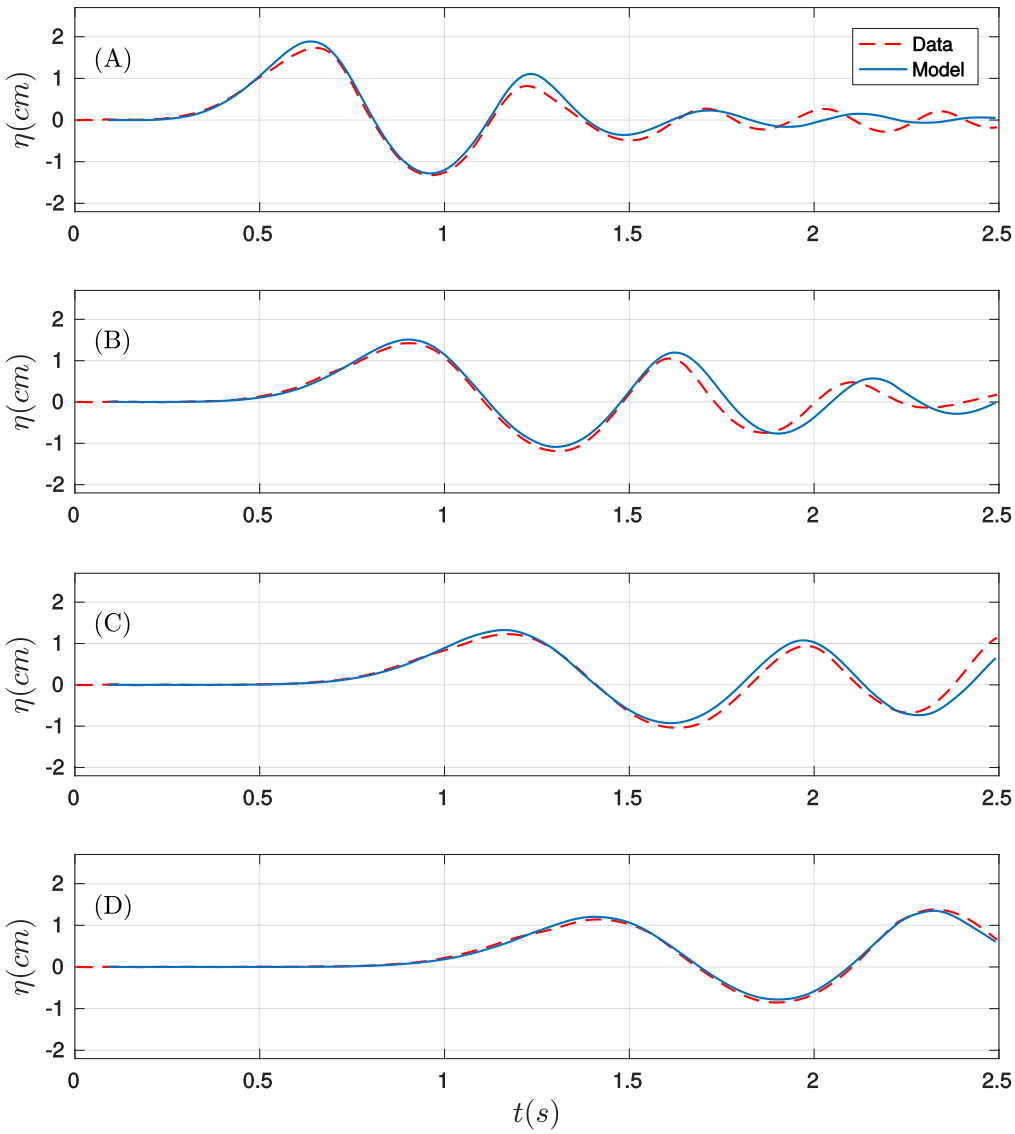

Figure 12: Comparison of data time series (red) and numerical (blue). Case 1. (A) G1, (B) G2, (C) G3, and (D) G4

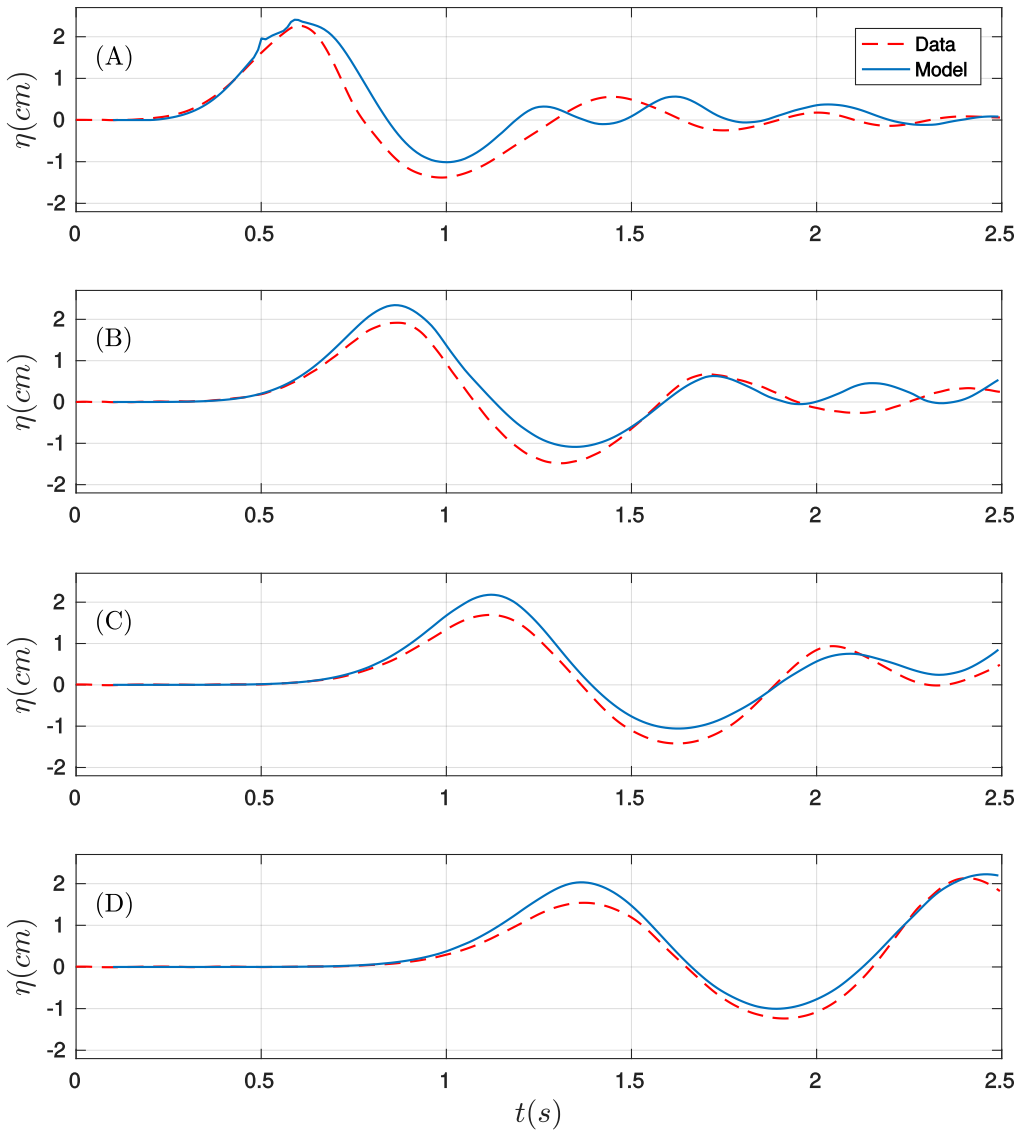

Figure 13: Comparison of data time series (red) and numerical (blue). Case 2. (A) G1, (B) G2, (C) G3, and (D) G4

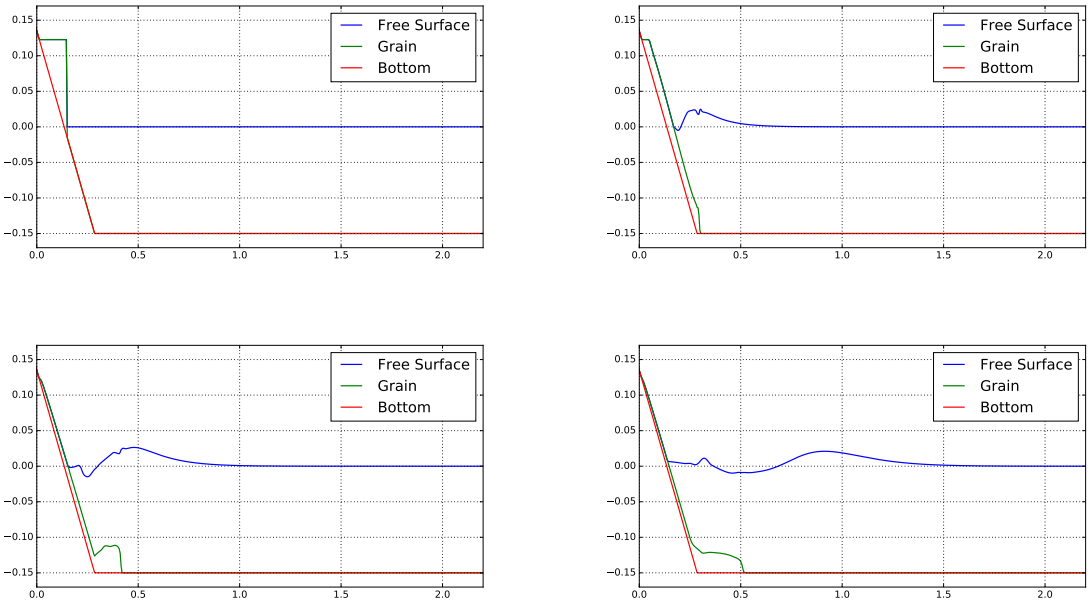

Figure 14: Numerical profiles of the water free surface elevation and the grain layer at times $t = 0,\ 0.2,\ 0.4,\ 0.8\ s$ for the Case 1.

4.6 Benchmark Problem 6: Three-dimensional subaerial granular slide

This benchmark problem is the only one we have not performed yet with any of the codes of the HySEA family. This will be done soon with the two-dimensional version of the same model used in the two previous benchmark problems, coupling the Multilayer-HySEA non-hydrostatic model with a Savage-Hutter model for the granular material. This code is currently under development.

4.7 Benchmark Problem 7: Field Case: Slide at Port Valdez, AK during 1964 Alaska Earthquake

The present benchmark consists on simulating the extent of the inundation for two slide events at Port Valdez (one at the head of the bay and another at the Shoup Bay Moraine), based on before and after bathymetry data, and performing a comparison of the simulated results with eye-witness observations of the event, and observed run-up distribution. We have performed simulations for 4 different scenarios, two consisting in single slide events: HPV (for Hotel Port Valdez) and SBM (for Shoup Bay Moraine); and two dealing with combined HPV/SBM scenarios, one using the same model parameters as for the single events initially simulated and a second one using new parameters to fit the combinedscenario to the observed data as a one single scenario. This latest case is the one better reproducing the described observed data.

4.7.1 HPV scenario

A range of model parameters has been considered in order to perform a large set of numerical simulations. The aim of this approach was to find the optimal values for the parameters considered (angle of repose, ratio of densities, friction between water and sediment and friction between water and bottom surface). In the case of HPV scenario, the parameters were taken in the following intervals:

- Angle of repose (α): $[4^o - 6^o]$

- Ratio of densities (fluidized sediment/water): $[0.25 - 0.45]$
- Friction water/sediment: $[0.005 - 0.01]$
- Friction water/bottom: 0.005

For this scenario the optimal parameters found were (among other posible choices):

- Angle of repose (α): 6.0
- Ratio of densities (fluidized sediment/water): 0.35
- Friction water/sediment: 0.005
- Friction water/bottom: 0.005

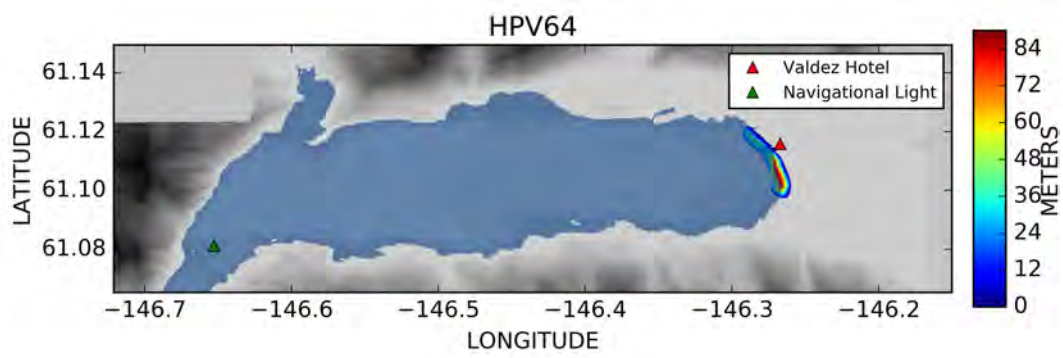

(a) HPV: Initial condition

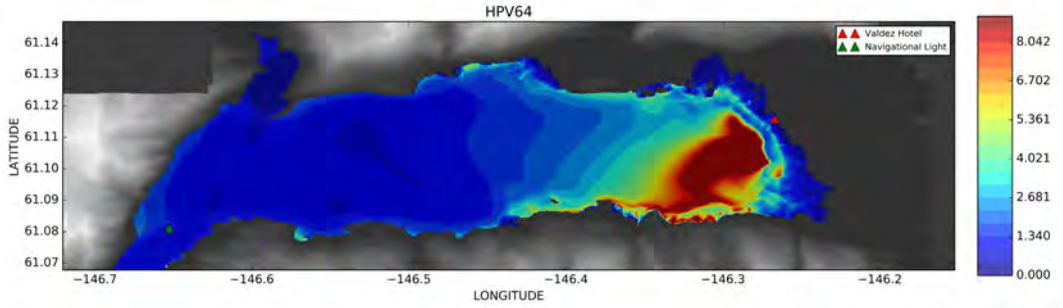

(b) HPV: Maximal free surface elevation

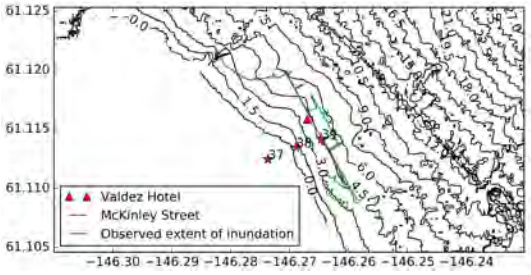

(c) Locations of selected points (37, 38, 39, and VH)

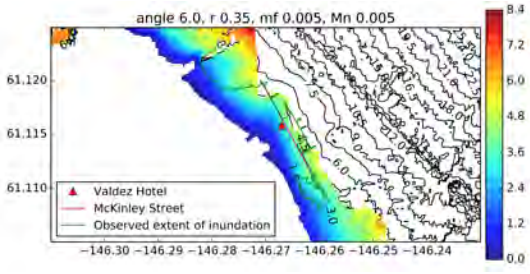

(d) Inundation at Valdez

Figure 15: HPV scenario

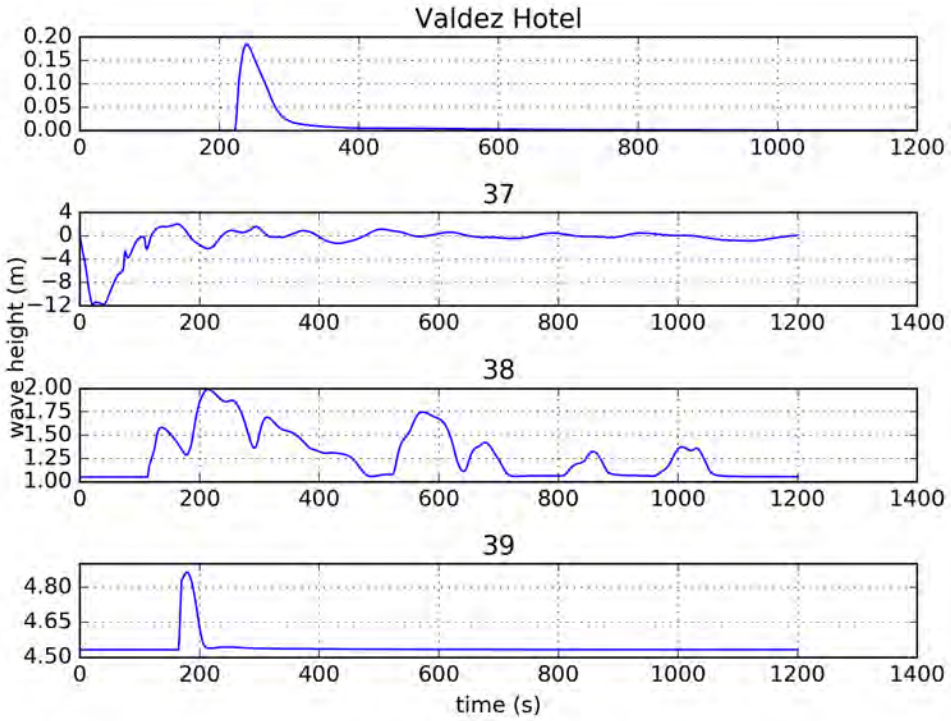

Figure 16: HPV scenario. Water elevation time series at Valdez locations

Figure 15.a shows the initial condition considered for this scenario, and Figure 15.b the maximum water surface elevation reached along the whole duration of the simulation. Figure 15.d presents the inundation extension at Valdez. It can be observed that McKinley Street is reached by the inundation. Figure 16 shows the time series of the water height at 4 selected locations at Valdez (shown in Figure 15.c), including Valdez Hotel. It can be observed that at location 38 several waves are numerically reproduced, but only one wave is observed at Valdez Hotel and location 39.

4.7.2 SBM scenario

In this second single slide scenario the varying intervals considered for the 4 model parameters were:

- Angle of repose (α): $[4^o - 9^o]$
- Ratio of densities (fluidized sediment/water): $[0.25 - 0.45]$
- Friction water/sediment: $[0.02 - 0.04]$
- Friction water/bottom: $[0.005 - 0.01]$

In this case the optimal parameters found were:

- Angle of repose (α): 5.0
- Ratio of densities (fluidized sediment/water): 0.45
- Friction water/sediment: 0.03
- Friction water/bottom: 0.005

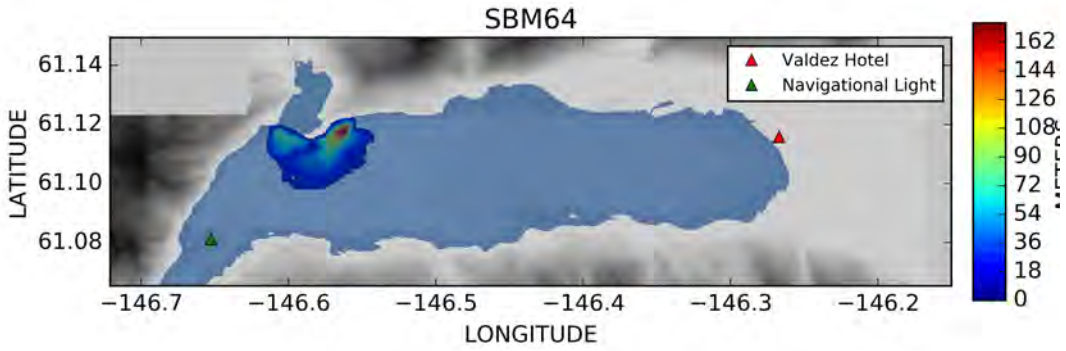

(a) SBM: Initial condition

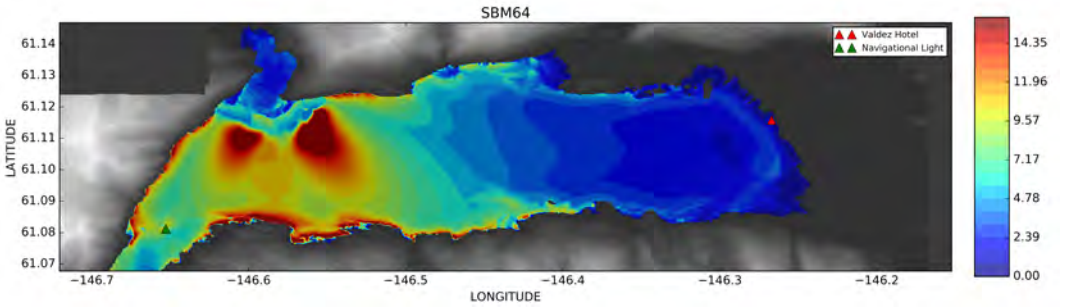

(b) SBM: Maximum free surface height

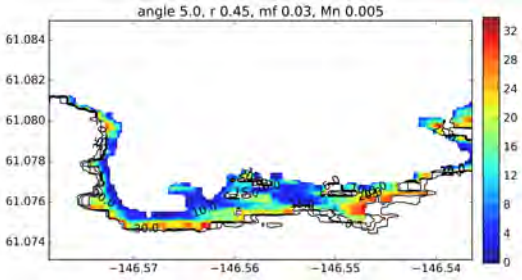

(c) Run-up at Anderson Bay

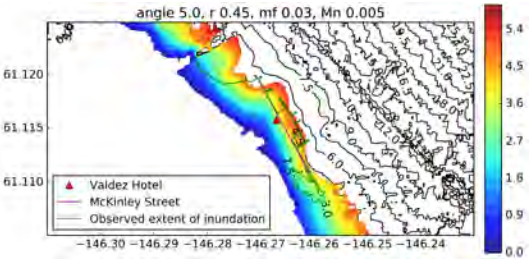

(d) Inundation at Valdez

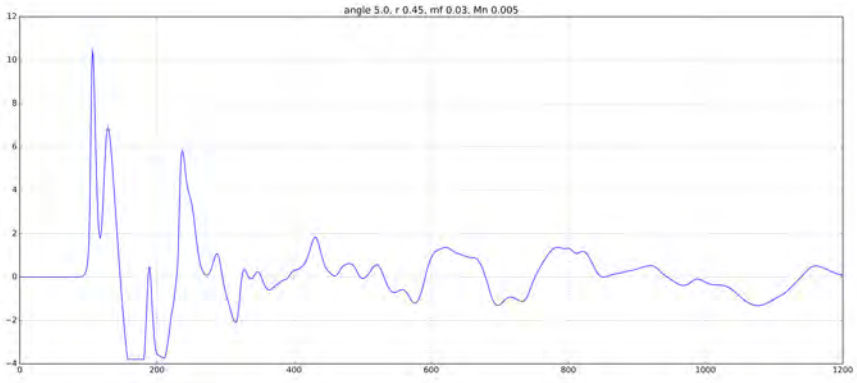

(e) HPV: Elevation time series at Navigational Light

Figure 17: SBM scenario

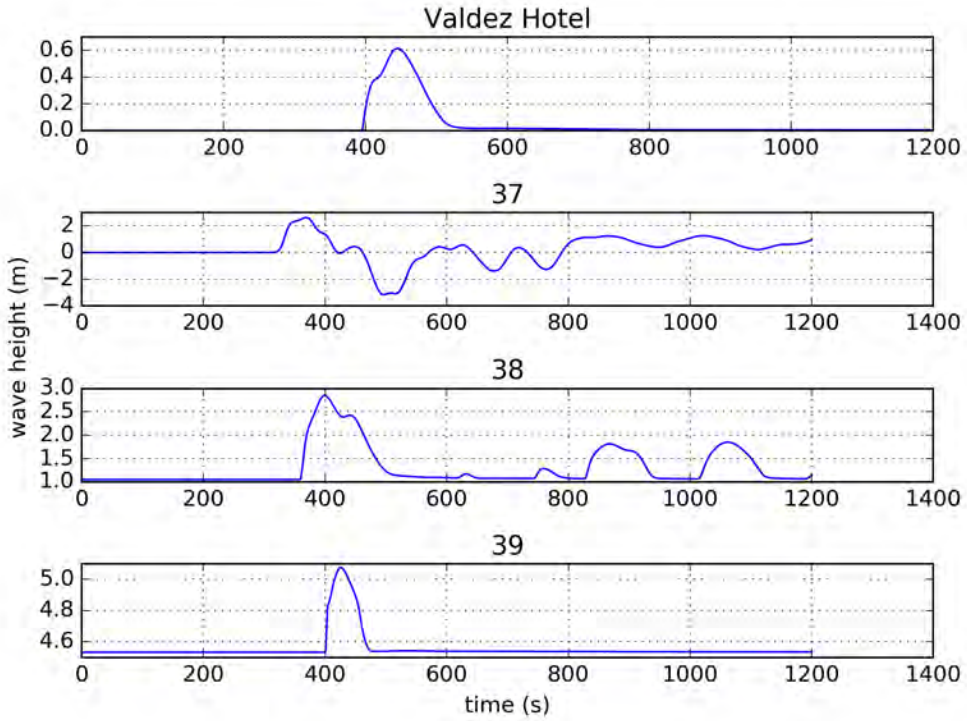

Figure 18: SBM scenario. Wave height time series at selected locations at Valdez

Figure 17.a shows the initial condition considered in this scenario, and Figure 17.b the maximum water surface elevation reached along the whole duration of the simulation. Figure 17.c depicts the run-up values computed for Anderson Bay (they are larger than 20 m). Figure 17.d presents the inundation around Valdez. It can be observed that McKinley street is reached by the inundation.

The wave height time series obtained at the navigation light is depicted in Figure 17.e, where a maximum value over is 10 m is obtained. Finally, in Figure 18 wave height time series at selected locations are depicted. A 60 cm wave arrive at Hotel Valdez, fulfilling the recommended benchmark objectives. It can be observed that at location 38 three waves are numerically reproduced, but only one wave is reproduced at Valdez Hotel and location 39.

4.7.3 SBM+HPV combined scenario

Now we consider a combined scenario, where both HPV and SBM slides are triggered simultaneously. As was the case for the two single scenarios, the combined scenario also fulfill the combination of all the required benchmark recommendations. Despite that this HPV+SBM combined scenario fulfills all the required items, we cannot consider this experiment setup optimal as, for example, in Anderson Bay numerical results do not fit accurately the observations.

The reason explaining this not optimal behavior is that, in the SMB case, it is recommended to reproduce 20+ m run-up at the Anderson Bay and an inundation larger than 0.5 m at Valdez Hotel. We do think that the requirement on the inundation at Valdez Hotel should be removed from SBM scenario and should be included in HPV case. The first argument to propose this change is that it seems to be more consistent that HPV slide be the main responsible of inundation at Valdez. Our second argument is based on the numerical simulations performed for the SBM case. We have observed that, when the reproduced inundation at Valdez Hotel reaches this 0.5 m value, the corresponding run-up at Anderson Bay is much larger than the real observed run-up of 20+ m (see Fig. 19 where 30+ m runup is simulated). This is also the reason for having an overestimated runup at Anderson Bay in

the combined scenario.

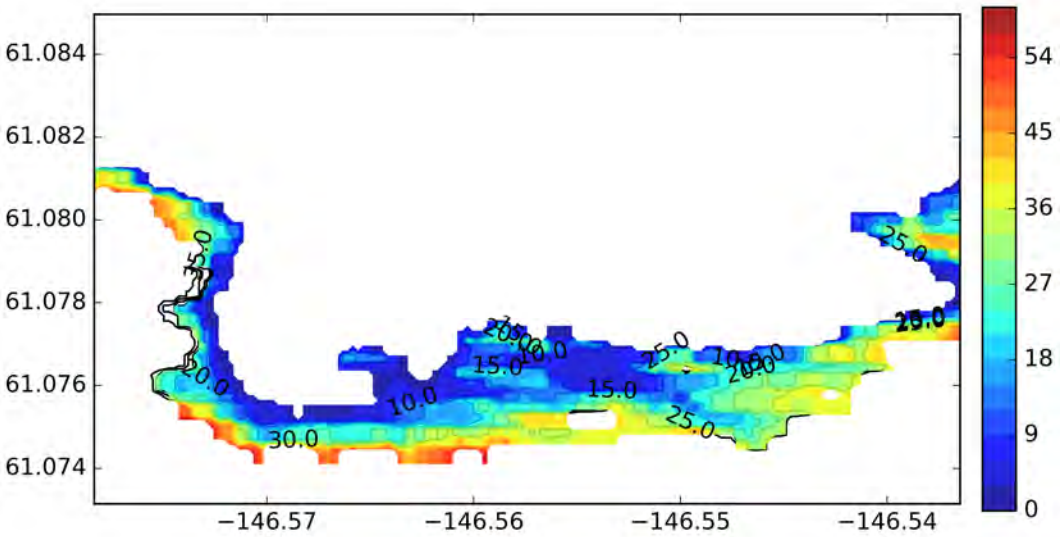

Figure 19: HPV+SBM combined scenario. Runup at Anderson Bay

Consequently, we have considered a new SBM* redefined experiment where we retain the condition over the run-up at the Anderson Bay, without trying to fulfill the condition on the inundation at Valdez Hotel, while we try to fulfill this last condition for the HPV scenario. The other requirements are retained as they were defined. Then, with the new parameters determined for SBM* scenario, a new combined scenario (named as HPV+SBM* combined experiment) has been considered. This numerical test fully achieves all the requirements while, at the same time, reproduces a better simulated runup at Anderson Bay than all previous scenarios.

Figure 20.a shows the inundation around Port Valdez as simulated in the optimal combined scenario. It can be observed that McKinley street is reached by the flooding wave. Figure 20.b depicts run-up values computed at Anderson Bay. Run-up values in this area are above 20 m. The wave-height time series reproduced at the Navigational Light is depicted at Figure 20.d. A maximum height over 12 m is obtained. Finally, Figure 21 presents the wave height time series of the combined scenario at the selected locations in Fig. 15.c compared with the two single scenarios, HPV and SBM*. It can be observed that, in the case of the combined scenario, two neat waves are simulated at Valdez Hotel and at location 39. They are separated by approximately 4 min. The first wave is 20 cm high, arriving to location 39 2.5 min after landslide triggering and about 4 min to Valdez Hotel. The second wave reaches more than 50 cm at Valdez Hotel arriving there 7 min after trigering. It is curious how, roughly speaking, the HPV component of the combined scenario is the responsible for the first simulated wave and while the second larger wave does not appear in the SBM scenario simulation. Therefore, this second wave is produced as result from the nonlinear combination of the waves produced by both slides occurring at the same time. The main discrepancy with the description provided for this combined scenario is the time between the two waves. The reported time is 10-15 min, while the simulated elapsed time at location 39 is around 5 min. The only way to obtained two waves separated by the reported time should be simulating two asynchronous slides separated by 5-10 min time. First the HPV slide and then, for example 5 min later, the SBM slide.

5 Acknowledgements

This research has been partially supported by the Spanish Government Research project SIMURISK (MTM2015-70490-C2-1-R and MTM2015-70490-C2-2-R) and the University of Málaga, Campus de

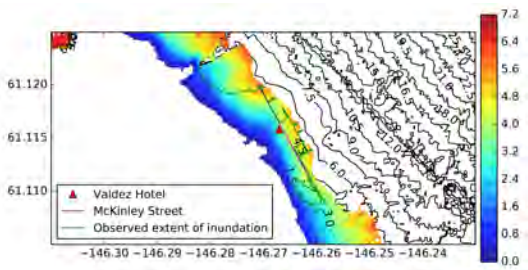

(a) HPV+SBM*: Inundation at Valdez

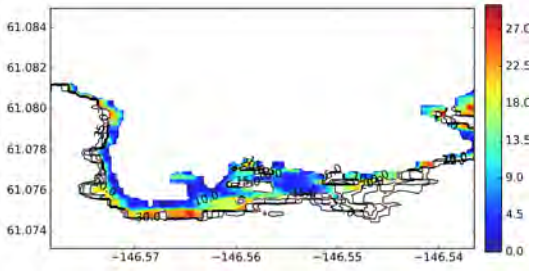

(b) HPV+SBM*: Run-up in Anderson Bay area

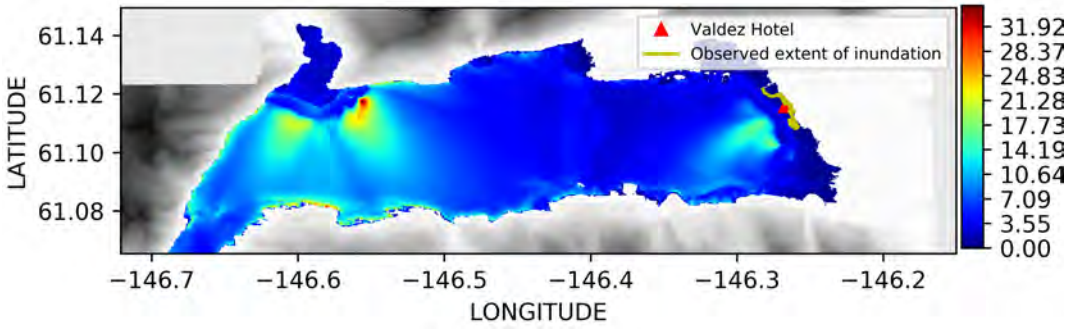

(c) Maximum wave height and inundation

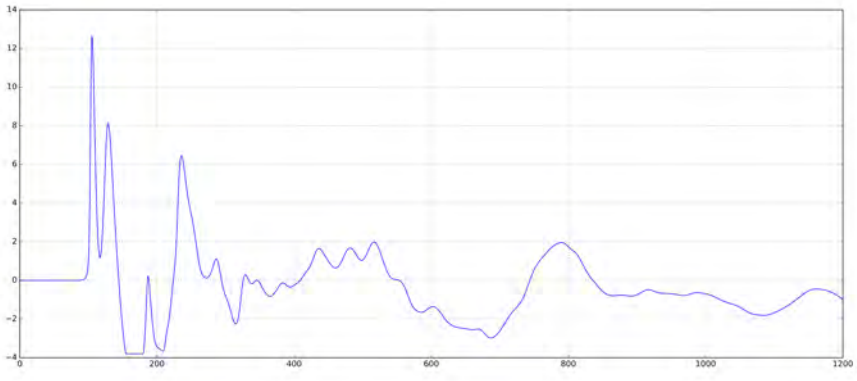

(d) Wave height time series at navigational gauge

Figure 20: HPV+SBM* (combined optimal) scenario

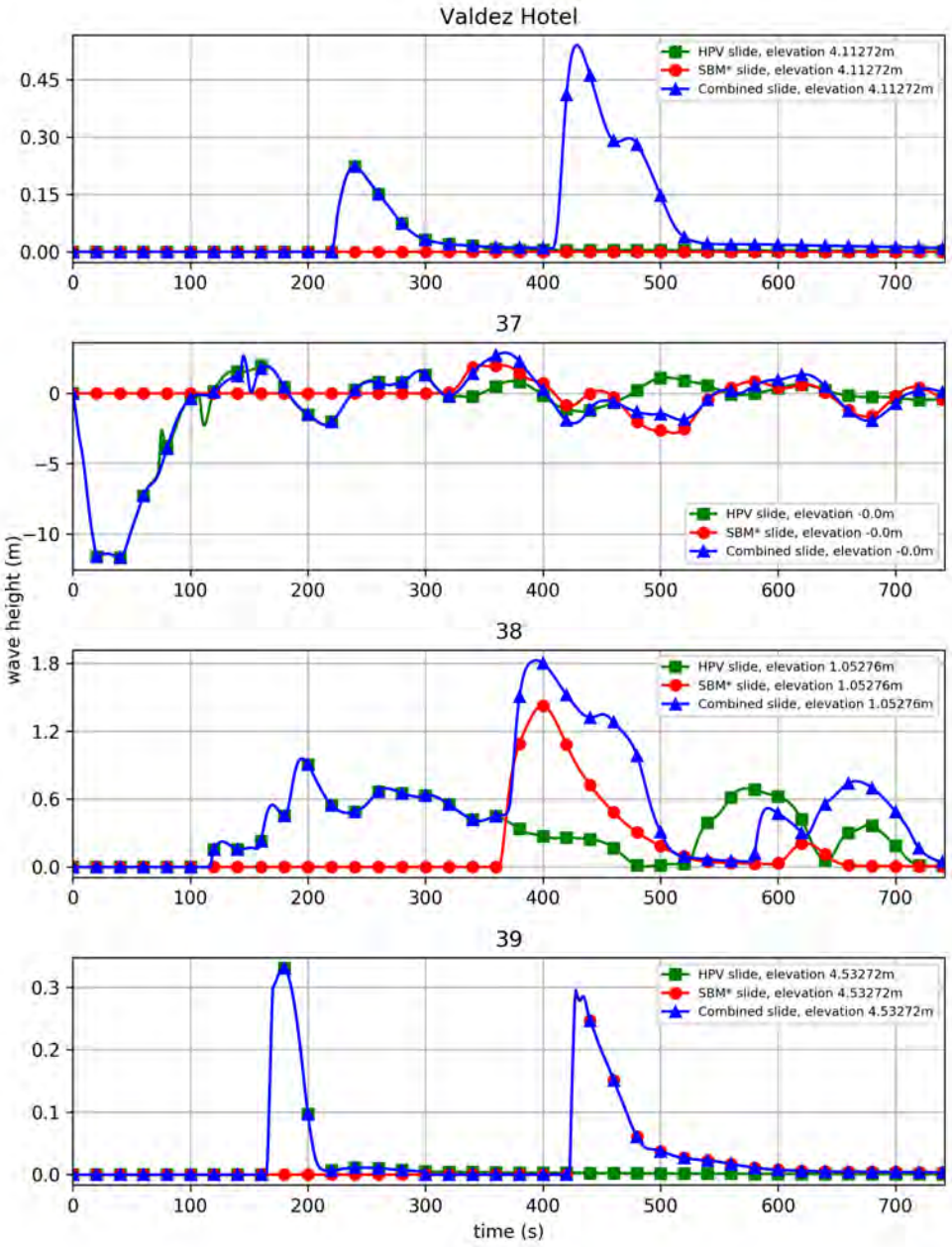

Figure 21: HPV+SBM* scenario. Wave height time series at selected locations. Comparison with HPV and SBM* scenarios

Excelencia Internacional Andalucía Tech. The multi-GPU computations were performed at the Unit of Numerical Methods (SCAI, University of Málaga).

References

[1] J.E. Adsuara, I. Cordero-Carrión, P. Cerdá-Durán, and M.A. Aloy. Scheduled relaxation Jacobi method: Improvements and applications. *Journal of Computational Physics*, 321:369–413, 2016.

[2] M.J. Castro, T. Chacón, E.D. Fernández-Nieto, J.M. González-Vida, and C. Parés. Well-balanced finite volume schemes for 2D non-homogeneous hyperbolic systems. Applications to the dam break of Aznalcóllar. *Comp. Meth. Appl. Mech. Eng.*, 197(45):3932–3950, 2008.

[3] M.J. Castro, E.D. Fernández-Nieto, J.M. González-Vida, and C. Parés. Numerical treatment of the loss of hyperbolicity of the two-layer shallow-water system. *J. Sci. Comput.*, 1(48):16–40, 2011a.

[4] M.J. Castro, A.M. Ferreiro, J.A. García, J.M. González, J. Macías, C. Parés, and M.E. Vázquez-Cendón. The numerical treatment of wet/dry fronts in shallow flows: Applications to one-layer and two-layer systems. *Mathematical and Computer Modelling*, 42(3–4):419–439, 2005.

[5] M.J. Castro, J.M. González, and C. Parés. Numerical treatment of wet/dry fronts in shallow flows with a modified Roe scheme. *Math. Mod. Meth. App. Sci.*, 16(6):897–931, 2006.

[6] M.J. Castro, S. Ortega, M. de la Asunción, J.M. Mantas, and J.M. Gallardo. GPU computing for shallow water flow simulation based on finite volume schemes. *Comptes Rendus Mécanique*, 339(2–3):165–184, 2011b.

[7] S. Cordier, M. Le, and T. Morales. Bedload transport in shallow water models: Why splitting (may) fail, how hyperbolicity (can) help. *Advances in Water Resources*, 8(34):980–989, 2011.

[8] M. de la Asunción, M.J. Castro, E.D. Fernández-Nieto, J.M. Mantas, S. Ortega, and J.M. González-Vida. Efficient GPU implementation of a two waves TVD-WAF method for the two-dimensional one layer shallow water system on structured meshes. *Computers & Fluids*, 80:441–452, 2013.

[9] M. de la Asunción, M.J. Castro, J.M. González-Vida, J. Macías, S. Ortega, and C. Sánchez-Linares. East coast non-seismic tsunamis: A first landslide approach. Technical report, NOAA report, 2013.

[10] M. de la Asunción, J.M. Mantas, and M.J. Castro. Evaluating the impact of cell renumbering of unstructured meshes on the performance of finite volume GPU solvers. In *12th International Conference on Computational and Mathematical Methods in Science and Engineering (CMMSE 2012)*, La Manga (España), Julio 2012, 2012.

[11] C. Escalante, T. Morales, and M.J. Castro. Non-hydrostatic pressure shallow flows: GPU implementation using finite–volume and finite–difference scheme. *Submitted to Applied Mathematics and Computation*, 2017.

[12] E.D. Fernández, F. Bouchut, D. Bresh, M.J. Castro, and A. Mangeney. A new Savage-Hutter type model for submarine avalanches and generated tsunami. *J. Comp. Phys.*, 227:7720–7754, 2008.

[13] E.D. Fernández-Nieto, M.J. Castro, and C. Parés. On an intermediate field capturing Riemann solver based on a parabolic viscosity matrix for the two-layer shallow water system. *Journal of Scientific Computing*, 48(1–3):117–140, 2011.

[14] E.D. Fernández-Nieto, M. Parisot, Y. Penel, and J. Sainte-Marie. Layer–averaged approximation of euler equations for free surface flows with a non–hydrostatic pressure. *hal–01324012*, 2016.

[15] D.J. Fritz, W.H. Hager, and H.-E Minor. Lituya Bay case: rockslide impact and wave runup. *Science of Tsunami Hazards*, 19(1):3–22, 2001.

[16] J.M. Gallardo, C. Parés, and M.J. Castro. On a well-balanced high-order finite volume scheme for shallow water equations with topography and dry areas. *J. Comput. Phys.*, 227(1):574–601, 2007.

[17] J.M. González-Vida, M. de la Asunción, M.J. Castro, J. Macías, S. Ortega, C. Sánchez-Linares, D. Arcas, and V. Titov. HySEA-Landslide GPU-based model: Validation to the 1958 Lituya Bay mega-tsunami. In Göcek (Turkey), editor, *International Tsunami Symposium (ITS2013)*, 2013. 25-28 September 2013.

[18] J.M. González-Vida, J. Macías, M.J. Castro, C. Sánchez-Linares, S. Ortega, and D. Arcas. The Lituya Bay landslide-generated mega-tsunami. Numerical simulation and sensitivity analysis. *Submitted to J. Geophys. Res.*, 2017.

[19] V. Heller and W.H. Hager. Waves types of landslide generated impulse waves. *Ocean Engineering*, 38(4):630–640, 2011.

[20] O. Iglesias. *Generación y propagación de tsunamis en el mar Catalano-Balear*. PhD thesis, Universitat de Barcelona, [http:/hdl.handle.net/2445/68704], 2015.

[21] O. Iglesias, G. Lastras, J. Macías, J.M. González-Vida, J.L. Casamor, S. Costa, and M. Canals. Analysis of the tsunamigenic potential of four submarine landslides located on the ibiza channel, western mediterranean sea. *In progress*, 2017.

[22] L. Jiang and P.H. LeBlond. The coupling of a submarine slide and the surface waves which it generates. *Journal of Geophysical Research: Oceans*, 97(C8):12731–12744, 1992.

[23] G. Ma, F. Shi, and J.T. Kirby. Shock-capturing non-hydrostatic model for fully dispersive surface wave processes. *Ocean Modelling*, 43–44:22–35, 2012.

[24] J. Macías, M.J. Castro, J.M. González-Vida, S. Ortega, and M. de la Asunción. HySEA tsunami GPU-based model. Application to FTRT simulations. In Göcek (Turkey), editor, *International Tsunami Symposium (ITS2013)*, 2013. 25-28 September 2013.

[25] J. Macías, M.J. Castro, S. Ortega, C. Escalante, and J.M. González-Vida. Performance benchmarking of Tsunami-HySEA model for NTHMP's inundation mapping activities. *Pure and Applied Geophysics*, 2017a.

[26] J. Macías, C. Escalante, and M.J. Castro. Performance assessment of Tsunami-HySEA model for NTHMP tsunami currents benchmarking. Part I Lab data. *Submitted to Coastal Engineering*, 2017b.

[27] J. Macías, S. Ortega, J.M. González-Vida, and M.J. Castro. Performance assessment of Tsunami-HySEA model for NTHMP tsunami currents benchmarking. Part II Field data. *Submitted to Coastal Engineering*, 2017c.

[28] J. Macías, J.T. Vázquez, L.M. Fernández-Salas, J.M. González-Vida, P. Bárcenas, M.J. Castro, V. Díaz del Río, and B. Alonso. The Al-Borani submarine landslide and associated tsunami. A modelling approach. *Marine Geology*, 361:79 – 95, 2015.

[29] C. Sánchez-Linares. Simulación numérica de tsunamis generados por avalanchas submarinas: aplicación al caso de Lituya Bay. Master's thesis, University of Málaga, Spain, 2011.

[30] S.B. Savage and K. Hutter. The motion of a finite mass of granular material down a rough incline. *J. Fluid Mech.*, 199:177–215, 1 1989.